Journal of the European Ceramic Society xxx (2017) xxx–xxx

Contents lists available at www.sciencedirect.com

Journal of the European Ceramic Society

journal homepage: www.elsevier.com/locate/jeurceramsoc

Effect of non-stoichiometry on the densification, phase purity, microstructure, crystal structure, and dielectric loss of $Ba(Co_{1/3}Nb_{2/3})O_3$ ceramics

Ahmad Sayyadi-Shahraki[a,b], Ehsan Taheri-Nassaj[a,*], Justin Gonzales[b], Nathan Newman[b], Taras Kolodiazhnyi[c]

[a] Department of Materials Science and Engineering, Tarbiat Modares University, Tehran, PO Box 14115-143, Iran
[b] Materials Program, Arizona State University, Tempe, Arizona 85287-6106, USA
[c] National Institute for Materials Science, 1-1 Namiki, Tsukuba, Ibaraki 305-0044, Japan

ARTICLE INFO

Article history:
Received 23 January 2017
Received in revised form 4 April 2017
Accepted 7 April 2017
Available online xxx

Keywords:
Dielectric loss
Sintering
Cation ordering
Microstructure
Point defects

ABSTRACT

The structural, vibrational, densification, and microwave properties of $Ba(Co_{1/3}Nb_{2/3})O_3$ ceramics with small compositional variations along several tie lines in the ternary BaO—CoO—Nb_2O_5 diagram were studied. The results showed that very small deviation from stoichiometric $Ba(Co_{1/3}Nb_{2/3})O_3$ composition has profound effect on $Q \times f$, degree of ordering, densification, and phase assemblage. The 0.94 $Ba(Co_{1/3}Nb_{2/3})O_3$–0.06 $Ba_5Nb_4O_{15}$ ceramic has the highest $Q \times f$ value (71 THz) – a value two times larger than that of stoichiometric $Ba(Co_{1/3}Nb_{2/3})O_3$ (36 THz). Transformation from the (partial) disordered distribution of Co and Nb cations to 1:2 ordered arrangement in the octahedral sites was found to increase the Q factor of the high density and single phase ceramics. It was also observed that formation of very small amount of $Ba_9CoNb_{14}O_{45}$ second phase degraded $Q \times f$ value severely for the dense and highly ordered Nb-rich and Ba-deficient ceramics.

1. Introduction

Ceramic dielectrics are used extensively in wireless communication technology. To maximize the performance of the systems, there are three important physical parameters of the materials that must be optimized; (*i*) dielectric loss tangent or its inverse, Q (the quality factor) >30,000 at 1 GHz, (*ii*) permittivity, $20 \leq \varepsilon_r \leq 50$, (*iii*) the temperature coefficient of resonant frequency of the microwave dielectric, $\tau_f = \frac{df}{fdT} \sim \pm 3 ppm/K$ [1].

The complex perovskite compounds with the formula $Ba\left(B'_{1/3}B''_{2/3}\right)O_3$ [where $B' = Zn, Mg, Co, Ni$ and $B'' = Ta$ and Nb] are commonly used in compact high performance wireless systems. Of these, $Ba(Zn_{1/3}Ta_{2/3})O_3$ (BZT) and $Ba(Mg_{1/3}Ta_{2/3})O_3$ (BMT) have impressive Q values of 14,000 at 12 GHz and 35,000 at 10 GHz, respectively and can have their τ_f tuned to zero by adding additives [2,3]. In spite of their desirable properties, the tantalum-reactants used to make BZT and BMT are expensive and the cost has become prohibitive for many commercial mobile systems [4]. For this reason, there is currently a significant amount of research being focused on achieving comparable or better performance in the less expensive niobate perovskites including $Ba(Zn_{1/3}Nb_{2/3})O_3$ (BZN), $Ba(Mg_{1/3}Nb_{2/3})O_3$ (BMN) and $Ba(Co_{1/3}Nb_{2/3})O_3$ (BCN).

Early efforts to understand the crystal structure of $Ba\left(B'_{1/3}B''_{2/3}\right)O_3$ compounds were conducted by Galasso et al. [5,6]. They reported that when a large charge or size difference exists between the B cations, the occupancy of the B site results in a 1:2 ordered structure along the (111) axis of the cubic unit cell (i.e. a sequence of $\{..B^{2+}B^{5+}B^{5+}B^{2+}B^{5+}B^{5+}..\}$). In the early work of Kawashima et al. [2] and Desu and O'Bryan [7], sintering BZT for an extended duration was found to increase the degree of B-site ordering and improve the microwave performance ($Q \times f$ > 165 THz).

The 1:2 ordered structure is stable below a thermodynamically-defined order-disorder transition temperature ($T_{o/d}$) [8–10]. Cation order is energetically favorable at the sintering temperature of the tantalates, while this is not true for the niobates. A very slow cooling rate (~2 K/h) from the sinter temperature or additional thermal processing below $T_{o/d}$ after sintering is required to form the 1:2 cation ordered structure. The $T_{o/d}$ of $Ba(Co_{1/3}Nb_{2/3})O_3$ compound is 1430 °C [11]. Thus, $Ba(Co_{1/3}Nb_{2/3})O_3$ ceramics that are furnace-cooled from the sintering temperature (~1400 °C) show poorly

* Corresponding author.
E-mail address: taheri@modares.ac.ir (E. Taheri-Nassaj).

http://dx.doi.org/10.1016/j.jeurceramsoc.2017.04.023
0955-2219/

ordered structure and quite low $Q \times f = 11$ THz [8]. Whereas, well-ordered $Ba(Co_{1/3}Nb_{2/3})O_3$ ceramics prepared with 1300 °C/12 h post-sintering anneals have $Q \times f$ products of 78 THz [12]. However, these values are still significantly below the intrinsic loss limit of $Q \times f \approx 150$ THz at $f = 90$ GHz inferred from whispering gallery mode measurements [13], indicating that the microwave performance of $Ba(Co_{1/3}Nb_{2/3})O_3$ ceramics are extrinsic loss limited.

As an alternative and more effective approach, the fabrication of samples with small deviations from stoichiometric $Ba\left(B'_{1/3}B''_{2/3}\right)O_3$ can produce samples with significant levels of 1:2 ordering. In 1993, Fujimaru et al. [14] found that $Q \times f$ could be enhanced by designing Mg-poor BMT compositions. A somewhat similar conclusion was also reported by studying Zn-deficient BZT and BZN ceramics [15–17]. Wu and Davis [15] proposed that the increase of 1:2 cation ordering in single phase dense BZN ceramics is responsible for the high $Q \times f$ product. However, more recently, Kolodiazhnyi [18] reported that Mg_{Ba} defects are the main source of extrinsic dielectric loss in highly ordered single phase ceramics. This suggests that a controlled deviation from the stoichiometry toward the B′-deficient compositions would lead to a drop in the B'_{Ba} concentration and thus increase in the $Q \times f$.

Other investigations of the influence of non-stoichiometry on the microwave performance of $Ba(Co_{1/3}Nb_{2/3})O_3$ ceramics have resulted in inconsistent conclusions. In the first report by Azough et al. [19], it was demonstrated that Co deficiency resulted in low-density high-loss materials. They were able to produce higher density Co-deficient materials using a V_2O_5 sintering agent, but this additive was found to degrade the Q-factor significantly. Later, Belous et al. [20] successfully prepared high-density ceramics along the $Ba_3CoNb_2O_9$ – $Ba_3Nb_2O_8$ tie line. Co-deficient ceramics, $Ba_3Co_{1+y}Nb_2O_{9+y}$ where $-0.1 \le y \le -0.05$, were obtained with $Q \times f$ values 30–50% higher than that found in $Ba(Co_{1/3}Nb_{2/3})O_3$. The influence of the $Ba(Co_{1/3}Nb_{2/3})O_3$ material properties in all possible directions of non-stoichiometry in the BaO-CoO-Nb_2O_5 ternary phase diagram has not been studied completely.

To resolve some of the unanswered questions from earlier investigations, we have carried out a study of a large number of compositions in the BaO-CoO-Nb_2O_5 phase diagram near the $Ba(Co_{1/3}Nb_{2/3})O_3$ compound. The phase purity and presence of secondary phases, the extent of 1:2 B-site cation ordering, the vibrational spectra, crystal structure distortion, density, microstructure and finally, microwave dielectric loss were determined.

2. Experimental procedure

Ceramic samples with the compositions summarized in Supplementary Information Table A were prepared by standard solid state method. High purity oxides and carbonate, Co_3O_4 (Sigma-Aldrich, 99.9%), Nb_2O_5 (Cerac, 99.99%) and $BaCO_3$ (Alfa Aesar, 99.9%) were used as the raw materials. These ingredients were dried at 300 °C for 15 h in air to remove absorbed water. An analytical balance with 0.1 mg accuracy was used to weigh the powder mixtures. A slurry was subsequently prepared by ball milling the mixture for 12 h in ethanol with yttrium-stabilized zirconia balls. Next, the slurry was dried and ground to fine powder. The mixtures of the raw materials were calcined at 1150 °C for 5 h in air. Then, the heated products were crushed into powder using agate mortar and pestle and milled again under the same condition that was used before. After drying, a small amount of 5% polyvinyl alcohol aqueous solution was added as a binder and the powders were thoroughly mixed and then screened through the 60-mesh sieve. Green cylindrical pellets of 7 mm diameter and 3.5 mm height were pressed under 115 MPa uniaxial pressure. Sintering was performed at 1400–1550 °C on alumina substrates coated with Y_2O_3 powder for 10 h with normal heating/cooling rates of 300 °C/h and 180 °C/h, respectively.

In order to study the effect of non-stoichiometry on the microwave dielectric loss in the $Ba(Co_{1/3}Nb_{2/3})O_3$ system, 40 compositions on 11 different binary tie lines, including $Ba(Co_{1/3}Nb_{2/3})O_3$-BaO (BaO excess, BCN2-BCN4), $Ba(Co_{1/3}Nb_{2/3})O_3$-$CoNb_2O_6$ (BaO deficiency, BCN5-BCN7), $Ba(Co_{1/3}Nb_{2/3})O_3$-CoO (CoO excess, BCN8-BCN12), $Ba(Co_{1/3}Nb_{2/3})O_3$-$Ba_3Nb_2O_8$ (CoO deficiency, BCN13-BCN15), $Ba(Co_{1/3}Nb_{2/3})O_3$-Nb_2O_5 (Nb_2O_5 excess, BCN16-BCN18), $Ba(Co_{1/3}Nb_{2/3})O_3$-Ba_3CoO_4 (Nb_2O_5 deficiency, BCN19-BCN21), $Ba(Co_{1/3}Nb_{2/3})O_3$-$Ba_4Nb_2O_9$ (BCN22-BCN25), $Ba(Co_{1/3}Nb_{2/3})O_3$-$Ba_5Nb_4O_{15}$ (BCN26-BCN28), $Ba(Co_{1/3}Nb_{2/3})O_3$-$BaNb_2O_6$ (BCN29-BCN32), $Ba(Co_{1/3}Nb_{2/3})O_3$-$Ba_2CoNbO_{5.5}$ (BCN33-BCN37) and $Ba(Co_{1/3}Nb_{2/3})O_3$-$Co_4Nb_2O_9$ (BCN38-BCN41) along with stoichiometric $Ba(Co_{1/3}Nb_{2/3})O_3$ (BCN1) composition, were prepared in the BaO-CoO-Nb_2O_5 ternary diagram. Fig. 1 indicates target sample compositions (black dots) in the BaO-CoO-Nb_2O_5 phase diagram. Optimized sintering temperatures and corresponding relative density values for each series of samples are summarized in Fig. 1 and Supplementary Information Table B.

The nature of primary and secondary phases and unit cell parameters of all sintered ceramics were analyzed using X-ray powder diffraction (Rigaku Ultima III X-ray diffractometer with Cu K_α X-ray source). Graphite crystal cut along the (0002) face was used to obtain monochromatic X-ray radiation. Rietveld refinement was performed using Jana 2006 software on all XRD data to infer the unit cell parameters and extent of 1:2 B-site ordering. Starting parameters for the refinement based on $P\bar{3}m1$ space group were taken from the Inorganic Crystal Structure Database, ICSD 150431, for partially ordered $Ba_3CoNb_2O_9$ structure [21]. The data were refined in the range of $10° \le 2\theta \le 140°$.

Atomic thermal factors, U_{iso}, were constrained to be equal for ions located on the same crystallographic site, i.e. $U_{iso}[Co(1b)] = U_{iso}[Nb(1b)]$ and $U_{iso}[Co(2d)] = U_{iso}[Nb(2d)]$. The U_{iso} value for O1(3e), O2(6i), and Co(1b) ions were fixed, while for Ba1(1a), Ba2(2d), and Nb(2d) were relaxed and refined to positive values. The fraction of Co ions occupying the 1b Wyckoff site (g[Co(1b)]) was used to deduce the extent of 1:2 cation ordering. For a fully ordered structure, the g[Co(1b)] = 100%, while it decreases to g[Co(1b)] = 33.3% for a completely random Co and Nb distribution in the B sites. The occupancy of the B sites were refined under the constraints $g[Co(1b)] \times 1 + g[Co(2d)] \times 2 = 1$ and $g[Nb(1b)] \times 1 + g[Nb(2d)] \times 2 = 2$, where g is the fractional occupancy of the ion whose Wyckoff site is shown in parentheses. All of the results were fit to a precision that resulted in R_p and GOF being close to 3% and unity, respectively.

Moreover, the deviation of the c/a ratio of the ordered trigonal structure from the $\sqrt{3/2} = 1.2247$ for the ideal undistorted cubic unit cell [22] was used as another gage for 1:2 cation ordering. Other indicators of ordering include the presence of superlattice diffraction peaks and splitting of high angle 420 into 422 and 226 reflections.

An XL30 ESEM-FEG scanning electron microscope was used to image the microstructural features of thermally etched surfaces in secondary electron and back scattered modes. Polished surfaces of samples were thermally etched at 100 °C below their sintering temperatures for 1 h. The chemical compositions of the grains were estimated by energy dispersive X-ray spectroscopy (EDS).

Raman spectra were collected from samples polished to a mirror surface using a custom built spectrometer in a 180° geometry with a 532 nm Coherent Sapphire SF laser. Laser power of 8 mW was focused on the samples in a 1–2 μm diameter spot and data was collected in the range of 50–1200 cm^{-1} with 30 s data point acquisition time with a spectral resolution of ~1 cm^{-1}.

For the microwave dielectric measurements, the ratio of the dielectric resonator's diameter to its thickness D/R was adjusted

Please cite this article in press as: A. Sayyadi-Shahraki, et al., Effect of non-stoichiometry on the densification, phase purity, microstructure, crystal structure, and dielectric loss of $Ba(Co_{1/3}Nb_{2/3})O_3$ ceramics, *J Eur Ceram Soc* (2017), http://dx.doi.org/10.1016/j.jeurceramsoc.2017.04.023

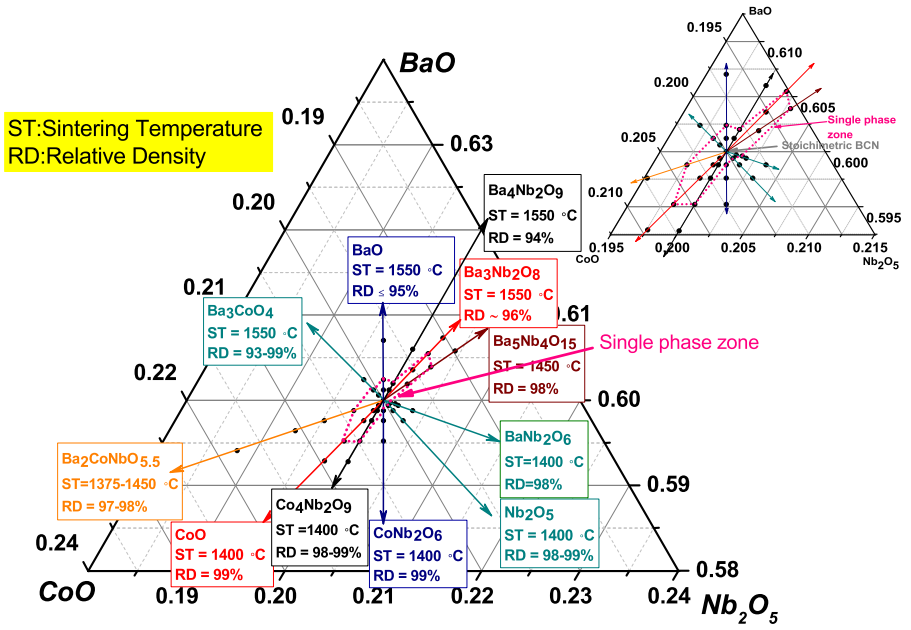

Fig. 1. Part of BaO-CoO-Nb_2O_5 ternary phase diagram in the vicinity of stoichiometric $Ba(Co_{1/3}Nb_{2/3})O_3$ composition. Small black dots on the binary lines indicate prepared compositions. Information included in each box shows optimized sintering temperature (ST) and calculated relative densities (RD) of the samples with compositions on the corresponding tie lines. Enclosed area with short dot-pink color lines around the stoichiometric $Ba(Co_{1/3}Nb_{2/3})O_3$ indicates the approximate single phase $Ba(Co_{1/3}Nb_{2/3})O_3$ zone. The inserted diagram on the upper-left side shows the zoomed single phase region.(For interpretation of the references to colour in this figure legend, the reader is referred to the web version of this article.)

to ≈2.26 to ensure that the first resonance mode is of the $TE_{01\delta}$-type. An HP8719C Vector Network Analyzer was used to measure the MW dielectric properties at frequencies of 9–10 GHz, except for the Ba-rich samples, BCN2 to BCN4 and BCN21. The dielectric properties of these porous samples could not be measured because no electromagnetic resonances were detected, presumably due to the high loss and/or low filling factor. The uncertainty in the determinations of the microwave dielectric parameters did not exceed 2%. The microwave measurements were performed according to the procedures described in Ref. [18].

3. Results and discussion

3.1. Dielectric properties

The compositional dependence of $Q \times f$ of the sintered ceramics is shown in Fig. 2. A summary of the microwave dielectric constant (ε_r), $Q \times f$, and resonant frequency (f_0) are also presented in Supplementary Information Table B. The stoichiometric BCN1 ceramics sintered at 1400 °C for 10 h exhibited a $Q \times f$ value of 36 THz. Studies in the literature [20,23,24] have reported $Q \times f$ values from 27 THz to 86 THz. It is not clear what might cause such a large scatter in reported values, although the differences in ceramic processing methods, purity of the raw chemicals, relative density, 1:2 cation ordering, and microstructural characteristics could have influenced the results [1]. In the study reported here, we synthesized samples with varying compositions using the same reactants, identical procedures, and the same equipment so that the results can be directly compared.

The $Q \times f$ value changes significantly even with slight deviations from stoichiometric $Ba(Co_{1/3}Nb_{2/3})O_3$. For ceramics with compositions on the $Ba(Co_{1/3}Nb_{2/3})O_3$–$Ba_5Nb_4O_{15}$ (BCN26-28) tie line, $Q \times f$ increased noticeably. For *(1-x)* $Ba(Co_{1/3}Nb_{2/3})O_3$–*x* $Ba_5Nb_4O_{15}$ ceramics, $Q \times f$ improves monotonically from 36 THz (BCN1) to 71 THz (BCN28) as x changed from 0 to 0.06, as shown in Fig. 2 and Supplementary Information Table B. However, for ceramic samples located in the Nb-rich and Ba-deficient regions, i.e. $Ba(Co_{1/3}Nb_{2/3})O_3$-$BaNb_2O_6$, $Ba(Co_{1/3}Nb_{2/3})O_3$-Nb_2O_5 and $Ba(Co_{1/3}Nb_{2/3})O_3$-$CoNb_2O_6$ tie lines, $Q \times f$ rises first and then decreases rapidly with further deviation from stoichiometry. For example, in the *(1-x)* $Ba(Co_{1/3}Nb_{2/3})O_3$–*x* $BaNb_2O_6$ ceramics, when the x value changes from 0 (BCN1) to $x = 0.005$ (BCN29), the $Q \times f$ is improved from 36.4 THz to 55.4 THz, then reduces sharply to 9.9 THz with further increase of x to 0.02. In the Co-rich regions, along the $Ba(Co_{1/3}Nb_{2/3})O_3$-CoO and $Ba(Co_{1/3}Nb_{2/3})O_3$-$Co_4Nb_2O_9$ tie lines, $Q \times f$ is smaller for the more Co-rich compositions when compared to the stoichiometric $Ba(Co_{1/3}Nb_{2/3})O_3$. This Q reduction is much more significant for the *(1-x)* $Ba(Co_{1/3}Nb_{2/3})O_3$–*x* $Co_4Nb_2O_9$ ceramics, as we can observe that the $x = 0.012$ compound possesses a $Q \times f$ value of only 17.6 THz. Similar trends were also found for the Ba-rich and Co/Nb-deficient ceramics found on the $Ba(Co_{1/3}Nb_{2/3})O_3$–Ba_3CoO_4, $Ba(Co_{1/3}Nb_{2/3})O_3$–BaO, $Ba(Co_{1/3}Nb_{2/3})O_3$-$Ba_4Nb_2O_9$ and $Ba(Co_{1/3}Nb_{2/3})O_3$-$Ba_3Nb_2O_8$ tie lines.

3.2. Structural characterization using X-ray diffraction analysis

All the sintered ceramics were studied using the X-ray powder diffraction technique to determine the presence of primary and potential secondary phases, degree of B-site cation ordering, and the unit cell lattice parameters. The solubility of native point defects was determined from both the SEM data and the evolution of the unit cell parameters as a function of deviation of the composition from $Ba(Co_{1/3}Nb_{2/3})O_3$ compound. According to Vegard's law, unit cell parameters of a continuous solid solution would vary linearly with composition for a substitutional solid solution [25]. As a result of Vegard's law, the solubility limit would be reached when the unit cell becomes invariant with further change in the composition of the solid solution [26]. This has proven to be an effective method to identify the formation of secondary phases when the concentration of a crystalline or amorphous secondary phase is below the detection limit of XRD analysis.

The single phase $Ba(Co_{1/3}Nb_{2/3})O_3$ region determined by this method, is revealed by short dot-pink color lines around the

Please cite this article in press as: A. Sayyadi-Shahraki, et al., Effect of non-stoichiometry on the densification, phase purity, microstructure, crystal structure, and dielectric loss of $Ba(Co_{1/3}Nb_{2/3})O_3$ ceramics, *J Eur Ceram Soc* (2017), http://dx.doi.org/10.1016/j.jeurceramsoc.2017.04.023

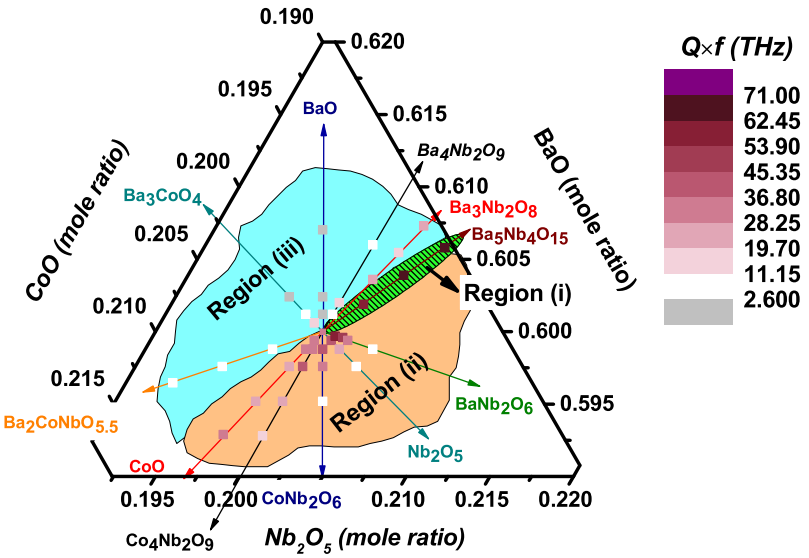

Fig. 2. The observed compositional dependence of $Q \times f$ for the BaO-CoO-Nb_2O_5 ternary phase diagram. The compositions near stoichiometric $Ba(Co_{1/3}Nb_{2/3})O_3$ were divided into three different sections; (i): green color filled with hatched pattern, (ii): orange color and (iii): blue color. (For interpretation of the references to colour in this figure legend, the reader is referred to the web version of this article.)

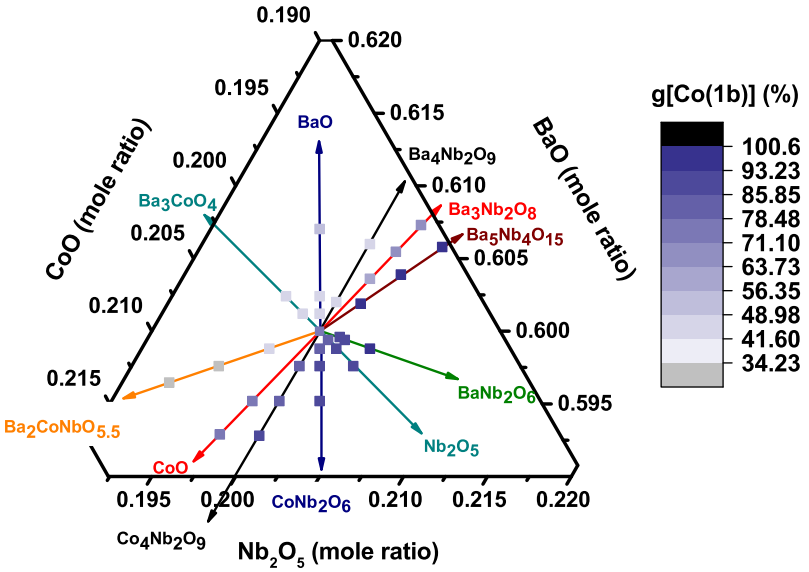

Fig. 3. The composition dependence in the degree of B site cation ordering, g[Co(1b)], for the studied ceramics in the BaO-CoO-Nb_2O_5 ternary phase diagram.

stoichiometric $Ba(Co_{1/3}Nb_{2/3})O_3$ in Fig. 1. The solubility limit in Ba/Nb-rich and deficient directions is much smaller than that in the Co-rich and deficient directions.

In the following, we present the values of the parameters determined from the X-ray diffraction measurements, g[Co(1b)] and c/a, in Figs. 3 and 4. More detailed data are given in Supplementary Information Table B. We can categorize the ceramics prepared in the present work into three categories based on their $Q \times f$ and 1:2 ordering (g[Co(1b)]) states as following:

(i) Ordering and high $Q \times f$; ceramics located on the $Ba(Co_{1/3}Nb_{2/3})O_3$-$Ba_5Nb_4O_{15}$ tie line.
(ii) Ordering and low $Q \times f$; ceramics located on $Ba(Co_{1/3}Nb_{2/3})O_3$-$BaNb_2O_6$, $Ba(Co_{1/3}Nb_{2/3})O_3$-Nb_2O_5, $Ba(Co_{1/3}Nb_{2/3})O_3$-$CoNb_2O_6$, $Ba(Co_{1/3}Nb_{2/3})O_3$-$Co_4Nb_2O_9$, and BCN-CoO tie lines.
(iii) Disordering and low $Q \times f$; ceramics located on $Ba(Co_{1/3}Nb_{2/3})O_3$-$Ba_2CoNbO_{5.5}$, $Ba(Co_{1/3}Nb_{2/3})O_3$-Ba_3CoO_4, $Ba(Co_{1/3}Nb_{2/3})O_3$-BaO, $Ba(Co_{1/3}Nb_{2/3})O_3$-$Ba_4Nb_2O_9$, and $Ba(Co_{1/3}Nb_{2/3})O_3$-$Ba_3Nb_2O_8$ tie lines.

Regions (i), (ii) and (iii) are highlighted in Fig. 2 by green, orange and blue colors, respectively.

3.2.1. Ceramics in region (i)

An example of the results from the Rietveld refinement employed to determine the g[Co(1b)] value and lattice parameters for BCN28, located in region (i), are shown in Fig. 5. In the XRD profile, the main superlattice 100 reflection at $2\theta \sim 17.6$ degrees associated with formation of 1:2 cation ordering can be observed. Moreover, the small reflection peaks from the $Ba_5Nb_4O_{15}$ secondary phase were also detected in the XRD pattern.

The chemical composition of the ceramics is *(1-x)* $Ba(Co_{1/3}Nb_{2/3})O_3$-*x* $Ba_5Nb_4O_{15}$ where $x = 0$–0.06. Fig. 1 shows that the solubility limit of the point defects reached $x = 0.04$ before a second phase identified as $Ba_5Nb_4O_{15}$ formed during

Please cite this article in press as: A. Sayyadi-Shahraki, et al., Effect of non-stoichiometry on the densification, phase purity, microstructure, crystal structure, and dielectric loss of $Ba(Co_{1/3}Nb_{2/3})O_3$ ceramics, *J Eur Ceram Soc* (2017), http://dx.doi.org/10.1016/j.jeurceramsoc.2017.04.023

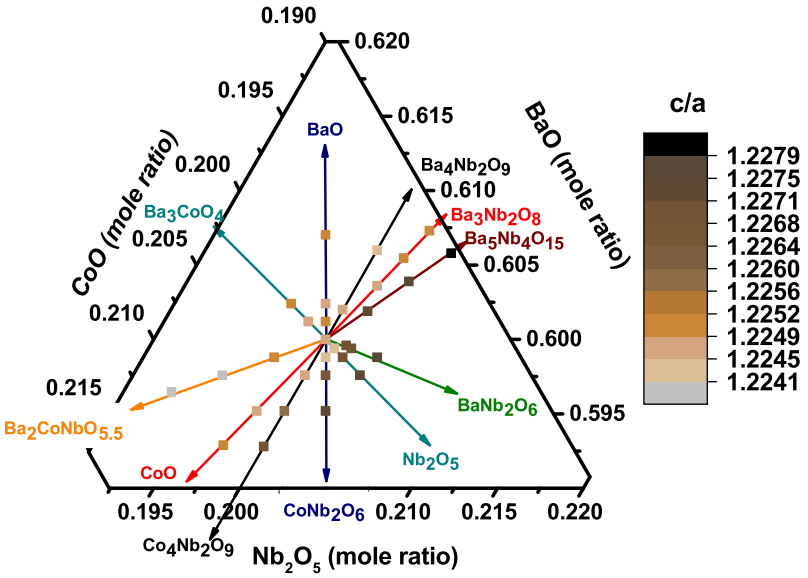

Fig. 4. The composition dependence of c/a parameter for the studied ceramics in the BaO-CoO-Nb_2O_5CoO ternary phase diagram.

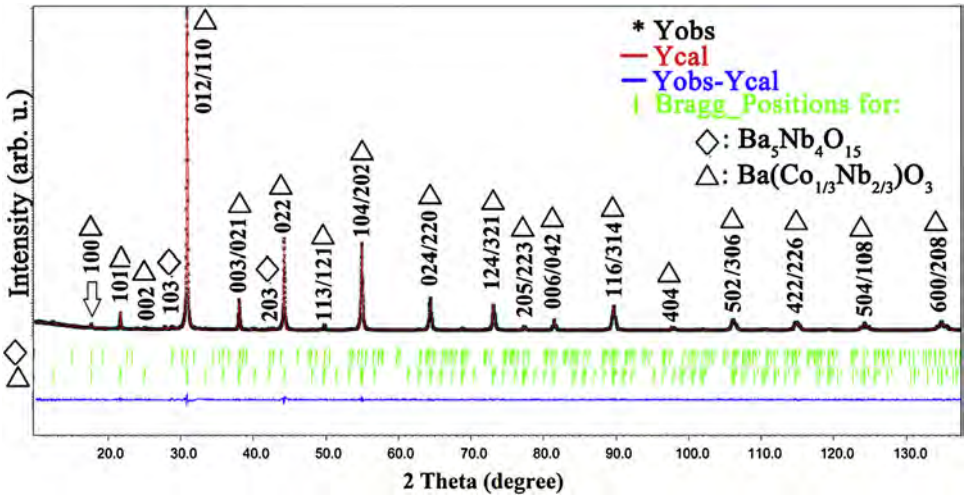

Fig. 5. The Rietveld refinement profile for sample BCN28. The asterisk symbols are the measured diffraction data. The calculated Rietveld profile is the red color line. The green vertical bars reveal the expected Bragg reflections and the difference between the observed and calculated data is depicted at the bottom of the plot in blue. The achieved R–factors for the refinement are GOF = 1.03, R_p = 2.90% and R_{wp} = 3.70%. The downward arrow indicates the 100 B-site order superlattice reflection. (For interpretation of the references to colour in this figure legend, the reader is referred to the web version of this article.)

the sintering process. The observed degree of B-site ordering, g[Co(1b)], for BCN1 (x = 0) 75(2)% was significantly smaller than 99(1)% for BCN28 (x = 0.06), as shown in Fig. 3. BCN28 sample's c/a ratio, another signature of 1:2 ordering, is also significantly larger (1.2280) than that of BCN1 (1.2247) sample. In fact, it is the largest value measured in this study (Fig. 4 and Supplementary Information Table B).

3.2.2. *Ceramics in region (ii)*

The ceramics located in this region show similar trends to that of region (i), i.e. the g[Co(1b)] value and c/a ratio increase with deviation from BCN1 composition.

As illustrated in Fig. 1, point defect solubility limit is very small for $Ba(Co_{1/3}Nb_{2/3})O_3$-$BaNb_2O_6$, $Ba(Co_{1/3}Nb_{2/3})O_3$-Nb_2O_5, $Ba(Co_{1/3}Nb_{2/3})O_3$-$CoNb_2O_6$ ceramics located in region (ii). X-ray diffraction results for the more Ba-deficient ceramic sample (BCN7) clearly indicate that the $Ba_9CoNb_{14}O_{45}$ phase with the tetragonal tungsten bronze structure (TTB) is present. The TTB secondary phase might be precipitated from a eutectic reaction during cooling from high temperature sintering (1400 °C). X-ray diffraction measurement results for Ba-deficient ceramics (BCN5 – BCN7) taken at low and high angles are shown in Fig. 6. Even though the XRD pattern of the BCN6 sample does not reveal any additional secondary phase peaks, the variation in the volume of the unit cell strongly suggests that a new phase is also present in this sample. Similarly, there are no detectable diffraction peaks associated with the secondary phase for the $Ba(Co_{1/3}Nb_{2/3})O_3$-$BaNb_2O_6$ and $Ba(Co_{1/3}Nb_{2/3})O_3$-Nb_2O_5 ceramics. However, as discussed below, based on the SEM and EDX observations, there is evidence that a secondary $Ba_9CoNb_{14}O_{45}$ phase might also be present in the $Ba(Co_{1/3}Nb_{2/3})O_3$-$BaNb_2O_6$ and $Ba(Co_{1/3}Nb_{2/3})O_3$-Nb_2O_5 samples.

The evolution of characteristics of B-site ordering (i.e. the 100 and 002 peaks in the low angle data and the splitting of the 420 reflection into 422 and 226 peaks in the high angle data), can be

Please cite this article in press as: A. Sayyadi-Shahraki, et al., Effect of non-stoichiometry on the densification, phase purity, microstructure, crystal structure, and dielectric loss of $Ba(Co_{1/3}Nb_{2/3})O_3$ ceramics, *J Eur Ceram Soc* (2017), http://dx.doi.org/10.1016/j.jeurceramsoc.2017.04.023

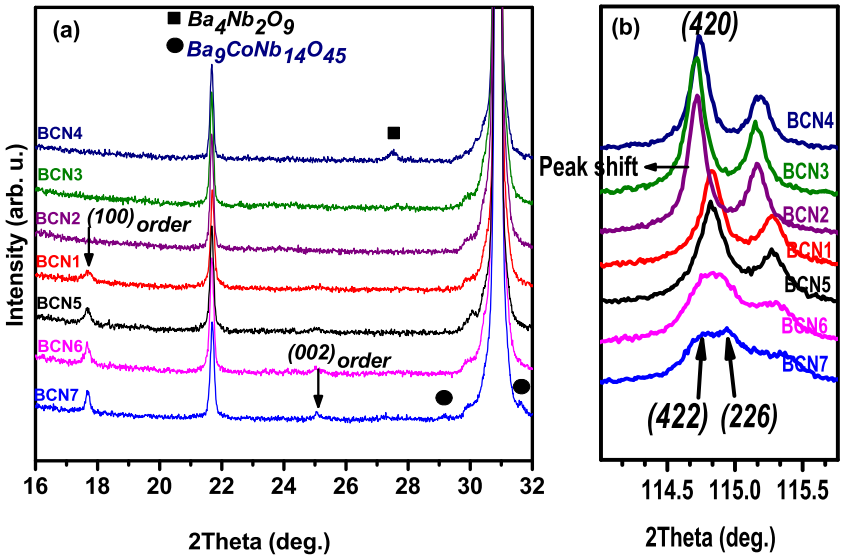

Fig. 6. X-ray diffraction data at (a) low and (b) high angles from Ba-deficient (BCN5 – BCN7) and Ba-excessive (BCN2 – BCN4) ceramics. The downward arrows show the superlattice ordering peaks. The solid square and two solid circles indicate the secondary phase reflections detected from BCN4 and BCN7, respectively.

clearly observed as one scans the X-ray diffraction data from BCN1 to BCN7. (Fig. 6).

The calculation of 1:2 cation ordering (g[Co(1b)]) shows that the extent of ordering was also improved for the $Ba(Co_{1/3}Nb_{2/3})O_3$-$Co_4Nb_2O_9$ and it was about the same as BCN1 for the $Ba(Co_{1/3}Nb_{2/3})O_3$-CoO ceramics. The most distinguishing aspect for these compositions is the much larger point defect solubility limit, as illustrated in Fig. 1.

3.2.3. Ceramics in region (iii)

All the ceramics located in region (iii) have a smaller degree of ordering (g[Co(1b)]) than that of BCN1 (Figs. 3 and 4) and they have a mostly disordered structure.

The XRD patterns of Ba-rich ceramics (BCN2–BCN4) are illustrated in Fig. 6. The presence of $Ba_4Nb_2O_9$ secondary phase was identified in *(1-x)* $Ba(Co_{1/3}Nb_{2/3})O_3$–*x* BaO, $x = 0.02$ (BCN4), ceramics. For the BCN2 and BCN3 ceramics, the shift in the 420 reflection toward smaller angles from that of the BCN1 sample indicates that the unit cell due to the incorporation of excess Ba cations, possibly as Ba'''_{Nb}, or Ba_{Co} antisite point defects, into the $Ba(Co_{1/3}Nb_{2/3})O_3$ lattice (Fig. 6(b)). For even higher Ba-rich sample, BCN4, the lattice did not expand further as a result of the formation of the $Ba_4Nb_2O_9$ secondary phase during sintering.

3.3. Raman spectroscopy

Fig. 7 illustrates the Raman spectroscopy data collected from mirror-smooth surfaces of the BCN1, $Ba(Co_{1/3}Nb_{2/3})O_3$-$Ba_5Nb_4O_{15}$ (BCN26-BCN28), $Ba(Co_{1/3}Nb_{2/3})O_3$-BaO (BCN2-BCN4) and $Ba(Co_{1/3}Nb_{2/3})O_3$-$CoNb_2O_6$ (BCN5-BCN7) ceramics. For BCN1, BCN26-BCN28 (Fig. 7(a)) and BCN5-BCN7 (Fig. 7(c)) ceramics, the measured spectra reveal four Raman active modes (i.e. $A_{1g(Nb)}$, $F_{2g(O)}$, $E_{g(O)}$ and $A_{1g(O)}$), whereas for Ba-rich ceramics, BCN2-BCN4 (Fig. 7(b)), only the $A_{1g(O)}$ band is observed. The presence of $F_{2g(O)}$ at 379 cm^{-1} and $A_{1g(O)}$ at 785 cm^{-1} in the Raman spectra are indicators of B-site ordering in complex perovskites. Furthermore, the observation of narrower line widths and higher intensities for these two bands is characteristic of enhanced levels of ordering [4,27]. The relative intensity of the $F_{2g(O)}$ peak as a function of deviation from the BCN1 composition is plotted in Fig. 7(d). The most intense $F_{2g(O)}$ band was found for the BCN28 sample and this was assigned a value of 100%. The relative intensities for all other samples were calculated using this as a reference.

The $F_{2g(O)}$ intensity, and thus the degree of long range B-site ordering, is found to systematically grow as the deviation from stoichiometry increases along the tie lines $Ba(Co_{1/3}Nb_{2/3})O_3$–$Ba_5Nb_4O_{15}$ and $Ba(Co_{1/3}Nb_{2/3})O_3$–$CoNb_2O_6$. However, the only Raman active mode in Ba-rich $Ba(Co_{1/3}Nb_{2/3})O_3$ samples observed is a broad and low intensity $A_{1g(O)}$ mode. These observations are consistent with our earlier results using Rietveld refinement of XRD data: cation ordering is enhanced for $Ba(Co_{1/3}Nb_{2/3})O_3$–$Ba_5Nb_4O_{15}$ and Ba-deficient compositions, while the Ba-rich ceramics possessed a disordered state.

3.4. Relative density and microstructural characteristics

All the compositions used in this study were sintered for 10 h at temperatures ranging from 1400 °C to 1550 °C. Fig. 8 shows the measured densities relative to the theoretical density as a function of composition. For BCN1 sample, a relative density of 99% was achieved at a sintering temperature of 1400 °C. The microstructure of the sintered BCN1 is revealed in Fig. 9(a). The grains with an average size of 2.1 μm are found to be closely packed without detectable signs of porosity.

For samples along the $Ba(Co_{1/3}Nb_{2/3})O_3$-$Ba_5Nb_4O_{15}$ tie-line (BCN26–BCN28), sintering temperatures higher than 1400 °C were needed to obtain high densities (Fig. 8 (a)). Sintering at 1450 °C resulted in a relative density of 98% with an average grain size of 0.9–1.1 μm. The SEM image of the BCN28 sample is illustrated in Fig. 9(b). The presence of grains with plate like shapes from a secondary phase can be found in the middle of equiaxed matrix grains in the SEM image. XRD analysis found the presence of a hexagonal $Ba_5Nb_4O_{15}$ perovskite as the secondary phase.

A sintering temperature of 1400 °C was sufficient to reach 98% relative density for the $Ba(Co_{1/3}Nb_{2/3})O_3$-$BaNb_2O_6$, $Ba(Co_{1/3}Nb_{2/3})O_3$-Nb_2O_5 and $Ba(Co_{1/3}Nb_{2/3})O_3$–$CoNb_2O_6$ ceramics located in region (ii). Increasing the temperature to 1450 °C did not increase the densification further (Fig. 8(a) and (b)). For all of these ceramics, new phases formed at very small deviations in stoichiometry. The formation of new phases were identified by microstructure images for all of the compositions with $x > 0.005$. Fig. 9(c) and (d) depicts the microstructure of *(1-x)*

Please cite this article in press as: A. Sayyadi-Shahraki, et al., Effect of non-stoichiometry on the densification, phase purity, microstructure, crystal structure, and dielectric loss of $Ba(Co_{1/3}Nb_{2/3})O_3$ ceramics, *J Eur Ceram Soc* (2017), http://dx.doi.org/10.1016/j.jeurceramsoc.2017.04.023

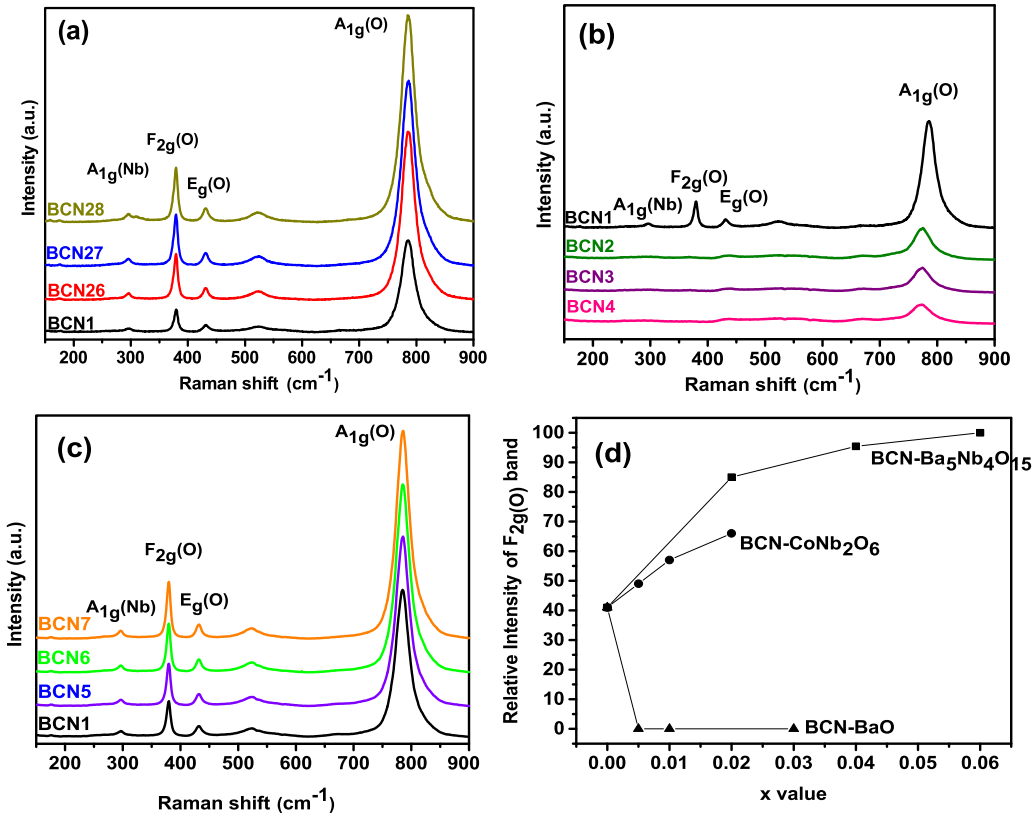

Fig. 7. Raman spectra for (a) $Ba(Co_{1/3}Nb_{2/3})O_3$-$Ba_5Nb_4O_{15}$ (BCN26-BCN28), (b) $Ba(Co_{1/3}Nb_{2/3})O_3$-BaO (BCN2-BCN4), and (c) $Ba(Co_{1/3}Nb_{2/3})O_3$-$CoNb_2O_6$ (BCN5-BCN7) ceramics. In order to compare to the stoichiometric composition, Raman spectrum of BCN1 ceramic is also presented in (a), (b), and (c). Relative intensities of $F_{2g(O)}$ band of the spectra are presented as a function of composition in (d).

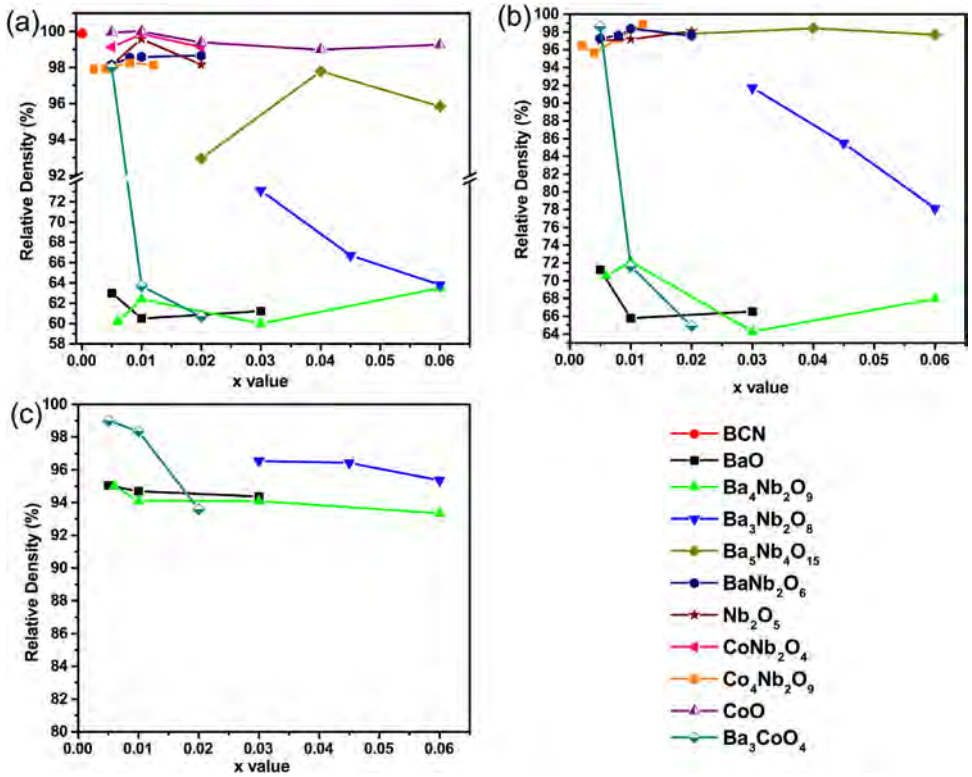

Fig. 8. Relative density as a function of composition variation for ceramics sintered at (a) 1400 °C, (b) 1450 °C and (c) 1550 °C. The legend associated with each composition is shown in the lower right side of Figure.

Please cite this article in press as: A. Sayyadi-Shahraki, et al., Effect of non-stoichiometry on the densification, phase purity, microstructure, crystal structure, and dielectric loss of $Ba(Co_{1/3}Nb_{2/3})O_3$ ceramics, *J Eur Ceram Soc* (2017), http://dx.doi.org/10.1016/j.jeurceramsoc.2017.04.023

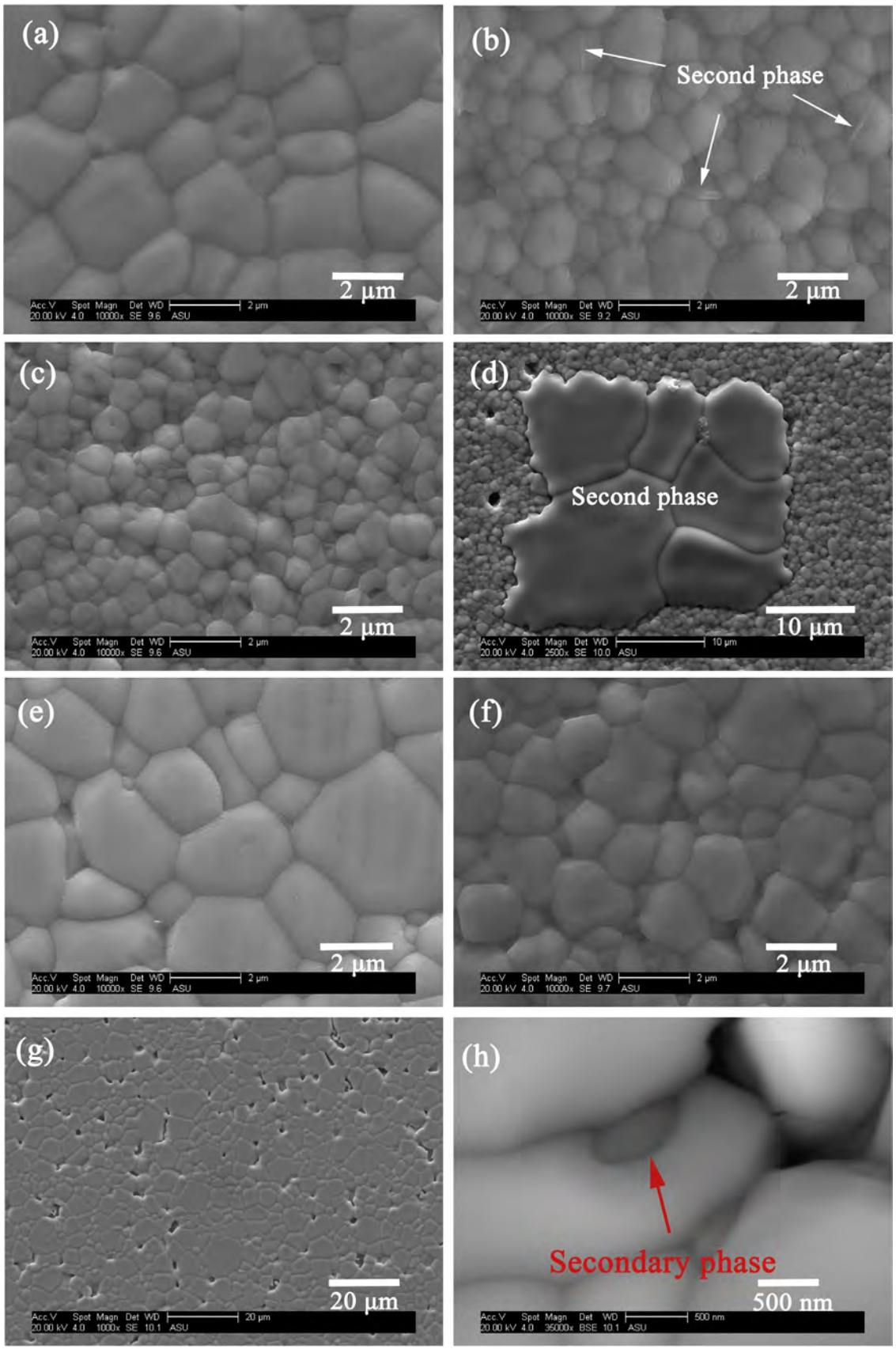

Fig. 9. The SEM images from thermally etched surfaces of (a) BCN1, (b) BCN28, (c) BCN16, (d) BCN18, (e) BCN11, (f) BCN40, (g) BCN4, and (h) backscatter image of BCN4 ceramics. Please note the different magnifications of the images.

Please cite this article in press as: A. Sayyadi-Shahraki, et al., Effect of non-stoichiometry on the densification, phase purity, microstructure, crystal structure, and dielectric loss of $Ba(Co_{1/3}Nb_{2/3})O_3$ ceramics, *J Eur Ceram Soc* (2017), http://dx.doi.org/10.1016/j.jeurceramsoc.2017.04.023

$Ba(Co_{1/3}Nb_{2/3})O_3$–x Nb_2O_5 ceramics for $x = 0.005$ (BCN16) and $x = 0.02$ (BCN18) sintered at 1400 °C, respectively. The former has closely packed $Ba(Co_{1/3}Nb_{2/3})O_3$ grains with an average size of 0.9 μm, while the BCN18 image shows the presence of a secondary phase with a much larger grain size (15 μm) than that of matrix phase. A similar coarse grain secondary phase was also observed for the $Ba(Co_{1/3}Nb_{2/3})O_3$-$BaNb_2O_6$ and $Ba(Co_{1/3}Nb_{2/3})O_3$-$CoNb_2O_6$ ceramics with the compositions outside of the single phase region. The composition of the secondary phase was determined by EDS to have atomic ratios of Nb/Ba = 1.6 and Co/Ba = 0.2. These values are within experimental error of the composition of the $Ba_9CoNb_{14}O_{45}$ compound identified by our XRD analysis.

The Co-rich $Ba(Co_{1/3}Nb_{2/3})O_3$-CoO (BCN8-BCN12) and $Ba(Co_{1/3}Nb_{2/3})O_3$-$Co_4Nb_2O_9$ (BCN38–BCN41) ceramics sintered at 1400 °C have relative densities of 98–99%, as illustrated in Fig. 8(a). The microstructural investigations of $Ba(Co_{1/3}Nb_{2/3})O_3$–CoO and $Ba(Co_{1/3}Nb_{2/3})O_3$-$Co_4Nb_2O_9$ revealed that in the former compounds, they have similar grain sizes (~2 μm) to that of BCN1, but the latter possessed smaller grain sizes (0.8–1.2 μm), as illustrated in Fig. 9(e) and (f), respectively.

The $Ba(Co_{1/3}Nb_{2/3})O_3$-BaO (Ba-rich), $Ba(Co_{1/3}Nb_{2/3})O_3$-Ba_3CoO_4 (Nb-deficient), $Ba(Co_{1/3}Nb_{2/3})O_3$–$Ba_3Nb_2O_8$ (Co-deficient), and $Ba(Co_{1/3}Nb_{2/3})O_3$-$Ba_4Nb_2O_9$ ceramics, located in region (iii), did not reach high sintering densities. Fig. 8 indicates that sintering at 1400 °C and 1450 °C produced ceramics with very low relative densities (70–80%). When the temperature was increased to 1550 °C, relatively dense ceramics (93–97%) were produced. The microstructure found in the SEM image of *(1-x)* $Ba(Co_{1/3}Nb_{2/3})O_3$–x BaO, $x = 0.03$ (BCN4) [Fig. 9(g)] has porosity and a large average grain size of 3.8 μm. The presence of the secondary phase $Ba_4Nb_2O_9$ was found in the grain boundary regions in the BCN4 ceramic, as shown in the backscatter image in Fig. 9(h).

In the following section, we will discuss how a small deviation from the $Ba(Co_{1/3}Nb_{2/3})O_3$ composition results in a noticeable variation in $Q \times f$. The *(1-x)* $Ba(Co_{1/3}Nb_{2/3})O_3$–x $Ba_5Nb_4O_{15}$ ceramic samples with $x < 0.04$ formed a single phase solid solution with $Q \times f$ much larger than BCN1 ceramic. For samples along this tie line, the relative densities and average grain size are decreased (Fig. 8(a, b)) with increasing deviation from BCN1, but the degree of B-site cation ordering, g[Co(1b)], and c/a ratio are enhanced. The crystal structure of stoichiometric BCN1 ($x = 0$) evolved from a partially ordered to fully ordered state for $x = 0.06$ (Figs. 3, 4 and 7(a)).

Identifying the mechanism for the increase in $Q \times f$ for $Ba(Co_{1/3}Nb_{2/3})O_3$-$BaNb_{4/5}O_3$ ceramics is of great scientific and practical importance. The solid solution chemical formula in this region can be written as $Ba\left(Co_{1-x}V''_{Co}{}_{0.6x}Nb^{\cdot\cdot\cdot\cdot}_{Co}{}_{0.4x}\right)_{1/3}Nb_{2/3}O_3$. It might be expected with the formation of the solid solution, Co vacancies and $Nb^{\cdot\cdot\cdot\cdot}_{Co}$ point defects are likely native point defects that could be present in such a material. However, the unit cell parameter for $Ba(Co_{1/3}Nb_{2/3})O_3$-$Ba_5Nb_4O_{15}$ solid solutions exhibited the lattice expansion over that of the BCN1 compound, a result inconsistent with the presence of a large density of V''_{Co} and $Nb^{\cdot\cdot\cdot\cdot}_{Co}$ point defects. The unit cell volume as a function of composition is plotted in Fig. 10. It can be seen with deviation from BCN1 ($x = 0$) toward BCN27 composition ($x = 0.04$) the lattice volume is increased from 204.839(8) Å^3 to 204.976(2) Å^3.

The formation of cobalt vacancies and partial substitution of the Co catoins ($r_{Co^{2+}} = 0.745$ *and* 0.65 Å for high and low spins, respectively) by smaller Nb^{5+} ($r_{Nb^{5+}} = 0.64$ Å) [28] would not be expected to result in lattice expansion. The accommodation of the excessive Nb^{5+} cations into interstitial sites ($Nb_i^{\cdot\cdot\cdot\cdot}$) might result in the lattice expansion but, the formation energy of cation Frenkel defects in closely packed complex perovskite is typically too high (6–8 eV) [18] to form in significant concentrations. Instead, the incorporation of large Ba cations with coordination number = 6

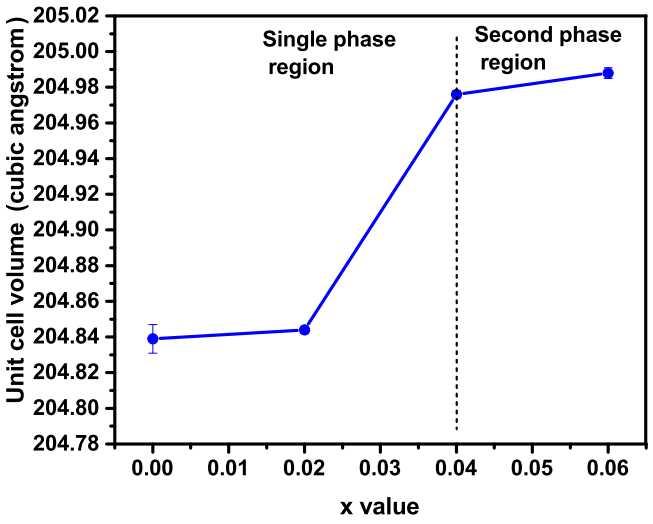

Fig. 10. The unit cell volume evolution as a function of composition (x) for $Ba(Co_{1/3}Nb_{2/3})O_3$-$Ba_5Nb_4O_{15}$ ceramics.

($r_{Ba^{2+}} = 1.35$ Å) [28] into Co site (Ba_{Co}) could be the possible reason for the unit cell expansion. The partial substitution of Ba cations for Zn sites due to Zn evaporation at high temperature in BZT ceramics was first proposed by Desu and O'Bryan [7].

As a result of partial Ba^{2+} transfer from A site to B' site of the perovskite, the average radii difference (Δr) between 2+ and 5+ ions at B site increases. According to Galasso et al. [29] and Bellaiche and Vanderbilt [30] the 1:2 ordering in the B site of A $\left(B'_{1/3}B''_{2/3}\right)O_3$ complex perovskites increases with the difference in the ionic radii between the B' and B" cations. Therefore, the improvement in the 1:2 cation ordering for $Ba(Co_{1/3}Nb_{2/3})O_3$–$Ba_5Nb_4O_{15}$ ceramics could be explained by the increased Δr as a result of the formation of Ba_{Co} point defects. Moreover, it was shown that the presence of $Ba_{B'}$ point defects could results in $Q \times f$ enhancement in fully ordered BZT ceramics by promoting further lattice distortion and subsequent c/a ratio deviation [7].

Our results and conclusions are generally consistent with other studies of $Ba(Mg_{1/3}Ta_{2/3})O_3$ and $Ba(Zn_{1/3}Nb_{2/3})O_3$ perovskite dielectrics. It was reported that the compositions on the $Ba_5Ta_4O_{15}$ and $Ba_5Nb_4O_{15}$ tie lines in the vicinity of stoichiometric BMT and BZN, respectively, possessed the highest Q factor [15,17]. However, in contrast to our conclusion, Wu and Davies [15] proposed that the 1:2 cation ordering and subsequent $Q \times f$ improvement in non-stoichiometric BZN system is a result of the dominance of V''_{Zn} point defect. In the case of non-stoichiometric BMT, the enhanced Q for the BMT- $Ba_5Ta_4O_{15}$ compositions was attributed to the formation of the crystal structure without oxygen vacancy defects [17]. Similarly, in the present study, the formation of BCN- $Ba_5Nb_4O_{15}$ solid solution with dominant Ba_{Co} point defects in the absence of the oxygen vacancies could also explain the enhanced $Q \times f$, since the presence of significant concentrations of oxygen vacancies prevents the 1:2 cation ordering and, thus, lowers the $Q \times f$ product [31].

Although BCN28 composition forms a fully 1:2 ordered and dense ceramic microstructure, the observed $Q \times f$ product (71 THz) is much smaller than the estimated intrinsic value (150 THz) from the whispering gallery mode studies [13]. Precipitation of $Ba_5Nb_4O_{15}$ secondary phase in BCN28 ceramic might have prevented achieving the high $Q \times f$ value expected for BCN ceramics.

Now, we will consider the compositions located in region (ii). For $Ba(Co_{1/3}Nb_{2/3})O_3$-$BaNb_2O_6$, $Ba(Co_{1/3}Nb_{2/3})O_3$-Nb_2O_5, $Ba(Co_{1/3}Nb_{2/3})O_3$-$CoNb_2O_6$ ceramics, it is observed that $Q \times f$ initially is enhanced and then markedly drops with increasing

Please cite this article in press as: A. Sayyadi-Shahraki, et al., Effect of non-stoichiometry on the densification, phase purity, microstructure, crystal structure, and dielectric loss of $Ba(Co_{1/3}Nb_{2/3})O_3$ ceramics, *J Eur Ceram Soc* (2017), http://dx.doi.org/10.1016/j.jeurceramsoc.2017.04.023

deviation from BCN1 composition. The solid solution chemical formula for *(1-x)* $Ba(Co_{1/3}Nb_{2/3})O_3$–*x* $BaNb_2O_6$ compositions in the single phase zone (Fig. 1) can be written as $Ba_{3-1.5x}Co_{1-x}Nb_xNb_2O_9$. The cation ordering parameter, g[Co(1b)], and c/a ratio increase due to enhanced B-site cation ordering and associated lattice distortion (Figs. 3 and 4). The solid solution $Ba_{3-1.5x}Co_{1-x}Nb_xNb_2O_9$ formula suggests that V''_{Ba} and $Nb^{\cdot\cdot\cdot}_{Co}$ point defects could potentially be present. It is expected that with the presence of V''_{Ba} and $Nb^{\cdot\cdot\cdot}_{Co}$ point defects, the unit cell would contract. Our determinations of the unit cell volumes are consistent with these suggestions, as it decreases from 204.839(8) Å^3 to 204.758(2) Å^3 for the 0.992 $Ba(Co_{1/3}Nb_{2/3})O_3$–0.008 $BaNb_2O_6$ solid solutions.

According to Wu and Davies [15,32], the presence of Ba vacancies could potentially enhance the degree of B-site cation ordering, as is the case when B′ vacancies are present. The presence of vacancies in the structure can enhance atomic diffusion in the lattice, promoting the formation of high quality, ordered crystals. It is also possible that the Ba vacancy could cause instability in the disordered structure by increasing the underbonded character of the O anions in the $B' - O - B'$ linkage that is only present in the disordered structure. We should note that the Ba vacancy formation could also influence the bonding nature of O ions in the ordered structure. However, in those structures, O anions are connected to at least one highly charged Nb cation that can move toward the O to mediate the adverse underbonded character [32].

The high density $Ba(Co_{1/3}Nb_{2/3})O_3$-Nb_2O_5 and $Ba(Co_{1/3}Nb_{2/3})O_3$-$CoNb_2O_4$ ceramics located in region (ii) showed the same behavior, i.e. their degree of cation ordering increases with increasing deviation from stoichiometry. The improvement in B-site cation ordering was determined using Rietveld refinement of the X-ray data (Figs. 3 and 4) and by the Raman spectroscopic analysis. The relative intensity of $F_{2g(O)}$ band, an indicator of long range cation ordering was enhanced in Ba-deficient $Ba(Co_{1/3}Nb_{2/3})O_3$ ceramics (Fig. 7(c) and (d)). However, the $Q \times f$ initially increased with increasing deviation from BCN1, but then dropped severely with increasing off-stoichiometry. For instance, $Q \times f$ first increased from 36 THz to 44 THz by changing *x* from 0 to 0.005, then, with further deviation from stoichiometry, it was reduced to 7 THz for 0.98 $Ba(Co_{1/3}Nb_{2/3})O_3$–0.02 $CoNb_2O_6$ (Ba-deficient ceramic). The drop in $Q \times f$ could be due to the formation of the secondary phase, as discussed in the following section.

It can be seen in Fig. 1 that $Ba(Co_{1/3}Nb_{2/3})O_3$-$BaNb_2O_6$, $Ba(Co_{1/3}Nb_{2/3})O_3$-Nb_2O_5, $Ba(Co_{1/3}Nb_{2/3})O_3$-$CoNb_2O_6$ compositions in region (ii) can only accommodate a small concentration of point defects before secondary phases form. It is observed for the $x > 0.005$ compositions, the secondary phase $Ba_9CoNb_{14}O_{45}$ forms at the same compositions that the $Q \times f$ is severely degraded.

It is clear that $A\left(B'_{1/3}B''_{2/3}\right)O_3$ complex perovskite compounds can only accommodate a small concentration of A-site vacancies before they form a secondary phase. The investigations of the $Ba(Mg_{1/3}Ta_{2/3})O_3$ and $Ba(Zn_{1/3}Ta_{2/3})O_3$ also showed that Ta-rich and Ba-deficient ceramics always contain secondary phase. For $Ba(Mg_{1/3}Ta_{2/3})O_3$ ceramics when moving from the $Ba(Mg_{1/3}Ta_{2/3})O_3$–$Ba_5Ta_4O_{15}$ tie line toward Ta-excessive and Ba-deficient regions, a Ta-rich compound identified as $Ba_9MgTa_{14}O_{45}$ was formed [18]. Moreover, Koga et al. [16] remarked that single phase material could not be synthesized for Ta-rich and Ba-deficient $Ba(Zn_{1/3}Ta_{2/3})O_3$. Similar observations have been reported for the Nb based complex perovskites $Ba(Zn_{1/3}Nb_{2/3})O_3$ and $Ba(Co_{1/3}Nb_{2/3})O_3$ [15,33,34]. Therefore, we conclude that the $Ba_9CoNb_{14}O_{45}$ tetragonal tungsten bronze phase was formed in our ceramics in region (ii). This particular phase exhibits typical relaxor ferroelectric behavior with a very high level of dielectric loss [35]. The existence of a small amount of this phase is responsible for a sharp decrease in $Q \times f$ for the dense and ordered Nb-rich and Ba-poor $Ba(Co_{1/3}Nb_{2/3})O_3$ samples in region (ii).

The $Ba(Co_{1/3}Nb_{2/3})O_3$-$Co_4Nb_2O_9$ and $Ba(Co_{1/3}Nb_{2/3})O_3$-CoO ceramics located in region (ii) contain excess Co and achieved densities of 98–99% after sintering at 1400 °C for 10 h *(1-x)* $Ba(Co_{1/3}Nb_{2/3})O_3$–*x* $Co_4Nb_2O_9$ ceramics formed a single phase solid solution for $x \leq 0.008$ and the *(1-x)* $Ba(Co_{1/3}Nb_{2/3})O_3$–*x* CoO could accommodate a significant number of point defects up until $x = 0.04$ (Fig. 1) without forming a secondary phase. In the single phase $Ba(Co_{1/3}Nb_{2/3})O_3$ region in this series, deviations from BCN1 along the $Co_4Nb_2O_9$ line resulted in an enhancement in the degree of B-site ordering g[Co(1b)] and yet a decline in $Q \times f$. When comparing the stoichiometric BCN1 sample to the single phase BCN40 sample, the 1:2 cation ordering increased from 75(2)% to 84(2)%, while the $Q \times f$ was reduced from 36.6 THz to 22.7 THz. One possibility for the degradation in $Q \times f$ is the decrease in grain size in the $Ba(Co_{1/3}Nb_{2/3})O_3$-$Co_4Nb_2O_9$ ceramics. However, it is not clear if this is a reasonable conclusion given that in the $Ba(Co_{1/3}Nb_{2/3})O_3$-$Ba_5Nb_4O_{15}$ ceramic series, the average grain size decreased, while the $Q \times f$ was enhanced significantly.

The dielectric loss anomaly was also observed for the Co-rich ceramics (along the $Ba(Co_{1/3}Nb_{2/3})O_3$-CoO tie line). The high density Co-rich BCN11 ceramic, which is located in the single phase region, possessed cation ordering and average grain size similar to that of stoichiometric BCN1. However, the $Q \times f$ decreased from 36.6 THz in the BCN1 to 27.4 THz in the Co-rich sample (BCN11). These results indicate that there might be an additional extrinsic source of dielectric loss in the Co-rich $Ba(Co_{1/3}Nb_{2/3})O_3$ compositions. Similar observations were reported by Kolodiazhnyi [18] in the study of $Ba(Mg_{1/3}Ta_{2/3})O_3$ system. In that study, the author found that $Q \times f$ dropped sharply for dense, highly ordered single phase Mg-rich ceramics. His experimental results revealed that by progressing from Mg-poor to Mg-rich compositions, the dominant point defect type would change from Ba_{Mg} to Mg_{Ba} species. It was suggested the rattling of Mg_{Ba} defects in the ac field could cause the high level of extrinsic dielectric loss. Similarly, rattling of the Co_{Ba} defect could cause the reduction of $Q \times f$ in the dense single phase Co-rich $Ba(Co_{1/3}Nb_{2/3})O_3$ ceramics, which have similar or higher levels of B-site cation ordering than the stoichiometric BCN1 sample.

Finally, all the compositions in region (iii) possessed very low $Q \times f$ values, even those located in a single phase $Ba(Co_{1/3}Nb_{2/3})O_3$ region. This includes Nb-deficient $Ba(Co_{1/3}Nb_{2/3})O_3$-Ba_4CoO_4, Ba-rich $Ba(Co_{1/3}Nb_{2/3})O_3$-BaO and $Ba(Co_{1/3}Nb_{2/3})O_3$-$Ba_4Nb_2O_9$, and Co-deficient $Ba(Co_{1/3}Nb_{2/3})O_3$–$Ba_3Nb_2O_8$ compositions. Relative density determinations and SEM studies (Figs. 8 and 9(g)) showed that all of these ceramics are porous. Even when these ceramics were sintered at 1550 °C, they did not attain the desired high densities. Therefore, the presence of pores could be the main reason for the observed low quality factors. It has been also reported that the addition of excessive Ba inhibits densification in the $Ba(Mg_{1/3}Ta_{2/3})O_3$ systems [36]. The point defect solubility limit for Ba-rich $Ba(Co_{1/3}Nb_{2/3})O_3$-BaO and $Ba(Co_{1/3}Nb_{2/3})O_3$-$Ba_4Nb_2O_9$ and Nb-deficient $Ba(Co_{1/3}Nb_{2/3})O_3$-Ba_3CoO_4 ceramics were very small and precipitation of impurity phases were detected. The presence of the $Ba_4Nb_2O_9$ phase was identified at the grain boundary region of Ba-rich ceramics, as illustrated in Fig. 9(h).

Furthermore, all of the Nb-deficient, Ba-rich and Co-deficient $Ba(Co_{1/3}Nb_{2/3})O_3$ ceramics located in region (iii) did not show evidence of significant ordering on the B-site in the XRD or Raman spectra (Fig. 7(b) and (d)). The highly disordered character of the Ba-rich ceramics could result from the substitution of excessive Ba into both Co and Nb sites simultaneously, that could reduce the average charge and size differences (Δq and Δr, respectively) between Co and Nb sites. Since the lower the Δq and Δr, the lower the driving force for B site cation ordering [29,30], this could be the root cause

Please cite this article in press as: A. Sayyadi-Shahraki, et al., Effect of non-stoichiometry on the densification, phase purity, microstructure, crystal structure, and dielectric loss of $Ba(Co_{1/3}Nb_{2/3})O_3$ ceramics, *J Eur Ceram Soc* (2017), http://dx.doi.org/10.1016/j.jeurceramsoc.2017.04.023

of our observations. By incorporation of larger Ba cations into the both B′ and B″ sites, the unit cell volume was expanded and is evident from high angle shift of the diffraction peak to lower 2θ (see results for BCN1 and BCN2 in Fig. 6(b)). In the case of Nb-deficient and Co-deficient ceramics, the formation of $V_{\ddot{O}}$ may contribute to loss of ordering. The formula for the Co-deficient $Ba(Co_{1/3}Nb_{2/3})O_3$-$Ba_3Nb_2O_8$ solid solution could be rewritten as $Ba_3Co_{1-x}Nb_2O_{9-x}$. Although, the introduction of Co vacancies could aid cation ordering, the existence of O vacancies significantly inhibits long range ordering [15,31,32].

In comparison to previous reports that investigated Co-deficient $Ba(Co_{1/3}Nb_{2/3})O_3$ ceramics, the results of this work showed that in these samples low $Q\times f$ values resulted from their poor sintering behavior and absence of long range 1:2 cation ordering. Our results are in agreement with Azough et al. [19] who reported that stoichiometric $Ba(Co_{1/3}Nb_{2/3})O_3$ had superior quality factor than the Co-deficient $Ba(Co_{1/3-x}Nb_{2/3})O_3$ $(0<x\leq 0.04)$ ceramics. This conclusion is different from Belous et al. [20] who reported that Co deficient ceramics, $Ba_3Co_{1+y}Nb_2O_{9+y}$, $-0.1\leq y\leq -0.05$ have superior $Q\times f$ values. However, because the $Ba(Co_{1/3}Nb_{2/3})O_3$-$Ba_3Nb_2O_8$ and BCN-$Ba_5Nb_4O_{15}$ tie lines are located so close to each other, small errors in chemical composition preparation procedure may bring the results of Belous et al. [20] in line with our conclusions for $Ba(Co_{1/3}Nb_{2/3})O_3$-$Ba_5Nb_4O_{15}$ ceramics.

4. Conclusions

Small deviations in stoichiometry of $Ba(Co_{1/3}Nb_{2/3})O_3$ ceramics resulted in large variations in the $Q\times f$ values in microwave dielectric loss. According to the observed $Q\times f$ changes and the 1:2 ordering calculations, the compositions around $Ba(Co_{1/3}Nb_{2/3})O_3$ were categorized into three groups. (i) Those located on the $Ba(Co_{1/3}Nb_{2/3})O_3$-$Ba_5Nb_4O_{15}$ tie line that showed significant improvements in $Q\times f$. The best $Q\times f$ value of 71 THz was achieved for the 0.94 $Ba(Co_{1/3}Nb_{2/3})O_3$-0.06 $Ba_5Nb_4O_{15}$ content, that is almost two times that of stoichiometric $Ba(Co_{1/3}Nb_{2/3})O_3$ (36 THz). The high levels of 1:2 B-site cation ordering was identified as the main reason for Q improvement. (ii) In the ordered Nb-rich, Ba-deficient, and Co-rich ceramics, the $Q\times f$ was degraded by the formation of the $Ba_9CoNb_{14}O_{45}$ TTB secondary phase for Nb-rich and Ba-deficient ceramics while the increased concentration of Co_{Ba} dipolar point defects might be the factor causing dielectric loss in Co-rich ceramics. (iii) Finally, for Nb-deficient, Ba-rich and Co-deficient compositions, the $Q\times f$ was decreased by deviation from the $Ba(Co_{1/3}Nb_{2/3})O_3$ composition due to the poor sintering behavior and absence of long range 1:2 cation ordering.

Acknowledgements

The use of facilities in the LeRoy Eyring Center for Solid State Science (LECSSS) at Arizona State University is acknowledged. A.S. thanks Prof. Vaclav Petricek for his useful advice on Rietveld refinement with Jana 2006 software. Collaboration between Dr. T. Kolodiazhnyi (NIMS) and Prof. N. Newman (ASU) was partially supported by Grant-in-Aid for Scientific Research 26400323 from JSPS.

Appendix A. Supplementary data

Supplementary data associated with this article can be found, in the online version, at http://dx.doi.org/10.1016/j.jeurceramsoc.2017.04.023.

References

[1] I.M. Reaney, D. Iddles, Microwave dielectric ceramics for resonators and filters in mobile phone networks, J. Am. Ceram. Soc. 89 (2006) 2063–2072.
[2] S. Kawashima, M. Nishida, I. Ueda, $Ba(Zn_{1/3}Ta_{2/3})O_3$ ceramics with low dielectric loss at microwave frequencies, J. Am. Ceram. Soc. 66 (1983) 421–423.
[3] K. Matsumoto, T. Hiuga, K. Takada, H. Ichimura, $Ba(Mg_{1/3}Ta_{2/3})O_3$ ceramics with ultra-low loss at microwave frequencies, Sixth IEEE International Symposium on Applications of Ferroelectrics (1986) 8–21.
[4] I. Reaney, Y. Iqbal, H. Zheng, A. Feteira, H. Hughes, D. Iddles, D. Muir, T. Price, Order–disorder behaviour in $0.9Ba([Zn_{0.60}Co_{0.40}]_{1/3}Nb_{2/3})O_3$–$0.1Ba(Ga_{0.5}Ta_{0.5})O_3$ microwave dielectric resonators, J. Eur. Ceram. Soc. 25 (2005) 1183–1189.
[5] F. Galasso, J.R. Barrante, L. Katz, Alkaline earth-tantalum-oxygen phases including the crystal structure of an ordered perovskite compound, $Ba_3SrTa_2O_9$, J. Am. Chem. Soc. 83 (1961) 2830–2832.
[6] F. Galasso, J. Pyle, Ordering in compounds of the $A(B'_{0.33}Ta_{0.67})O_3$ type, Inorg. Chem. 2 (1963) 482–484.
[7] S. Desu, H.M. O'Bryan, Microwave loss quality of $BaZn_{1/3}Ta_{2/3}O_3$ ceramics, J. Am. Ceram. Soc. 68 (1985) 546–551.
[8] I. Molodetsky, P. Davies, Effect of $Ba(Y_{1/2}Nb_{1/2})O_3$ and $BaZrO_3$ on the cation order and properties of $Ba(Co_{1/3}Nb_{2/3})O_3$ microwave ceramics, J. Eur. Ceram. Soc. 21 (2001) 2587–2591.
[9] P. Davies, H. Wu, A. Borisevich, I. Molodetsky, L. Farber, Crystal chemistry of complex perovskites: new cation-ordered dielectric oxides, Annu. Rev. Mater. Res. 38 (2008) 369–401.
[10] I. Reaney, I. Qazi, W. Lee, Order–disorder behavior in $Ba(Zn_{1/3}Ta_{2/3})O_3$, J. Appl. Phys. 88 (2000) 6708–6714.
[11] P.M. Mallinson, J.B. Claridge, M.J. Rosseinsky, R.M. Ibberson, J.P. Wright, A.N. Fitch, T. Price, D.M. Iddles, Cation ordering/disordering kinetics in $Ba_3CoNb_2O_9$: an in situ study using synchrotron X-Ray powder diffraction, Appl. Phys. Lett. 91 (2007) 222901.
[12] P. Mallinson, M. Rosseinsky, R. Ibberson, T. Price, D. Iddles, Processing control of phase separation, cation ordering, and the dielectric properties of $Ba_3(Co_{0.6}Zn_{0.4})Nb_2O_9$, Appl. Phys. Lett. 91 (2007) 2906.
[13] T. Kolodiazhnyi, G. Annino, T. Shimada, Intrinsic limit of dielectric loss in several $Ba(B'_{1/3}B''_{2/3})O_3$ ceramics revealed by the whispering-gallery mode technique, Appl. Phys. Lett. 87 (2005) 212908.
[14] Takuya Fujimaru, Masamitsu Nishida, Koichi Kugimiya. United States Patent 5,246,898.
[15] H. Wu, P.K. Davies, Influence of non-stoichiometry on the structure and properties of $Ba(Zn_{1/3}Nb_{2/3})O_3$ microwave dielectrics: II. compositional variations in pure BZN, J. Am. Ceram. Soc. 89 (2006) 2250–2263.
[16] E. Koga, Y. Yamagishi, H. Moriwake, K. Kakimoto, Ohsato H. Large, Q factor variation within dense, highly ordered $Ba(Zn_{1/3}Ta_{2/3})O_3$ system, J. Eur. Ceram. Soc. 26 (2006) 1961–1964.
[17] H. Ohsato, Microwave dielectrics with perovskite-type structure, in: L. Pan, G. Zhu (Eds.), Perovskite Materials-Synthesis, Characterisation, Properties, and Applications, INTEC, 2016, pp. 281–330.
[18] T. Kolodiazhnyi, Origin of extrinsic dielectric loss in 1: 2 ordered, single-phase $BaMg_{1/3}Ta_{2/3}O_3$, J. Eur. Ceram. Soc. 34 (2014) 1741–1753.
[19] F. Azough, C. Leach, R. Freer, Effect of nonstoichiometry on the structure and microwave dielectric properties of $Ba(Co_{1/3}Nb_{2/3})O_3$ ceramics, J. Eur. Ceram. Soc. 26 (2006) 2877–2884.
[20] A.G. Belous, O.V. Ovchar, A.V. Kramarenko, B. Jancar, J. Bezjak, D. Suvorov, Effect of nonstoichiometry on the structure and microwave dielectric properties of $Ba(Co_{1/3}Nb_{2/3})O_3$, Inorg. Mater. 46 (2010) 529–533.
[21] Inorganic Crystal Structure Database, Database code ICSD 150431: Fachinformationszentrum (FIZ) Karlsruhe. 2006.
[22] P.K. Davies, J. Tong, T. Negas, Effect of ordering-induced domain boundaries on low-loss $Ba(Zn_{1/3}Ta_{2/3})O_3$-$BaZrO_3$ perovskite microwave dielectrics, J. Am. Ceram. Soc. 80 (1997) 1727–1740.
[23] Z. Wang, J. Wu, L. Wang, Z. Fu, Q. Zhang, Effects of sintering process on microstructure and microwave dielectric properties of $Ba(Co_{1/3}Nb_{2/3})O_3$ ceramics, Electron. Mater. Lett. 10 (2014) 1121–1125.
[24] M. Li, A. Feteira, M. Mirsaneh, S. Lee, M.T. Lanagan, C.A. Randall, D.C. Sinclair, Influence of nonstoichiometry on extrinsic electrical conduction and microwave dielectric loss of $BaCo_{1/3}Nb_{2/3}O_3$ ceramics, J. Am. Ceram. Soc. 93 (2010) 4087–4095.
[25] A.R. Denton, N.W. Ashcroft, Vegard's law, Phys. Rev. A 43 (1991) 3161–3164.
[26] S. Hui, A. Petric, Electrical properties of yttrium-doped strontium titanate under reducing conditions, J. Electrochem. Soc. 149 (2002) J1–10.
[27] H. Zheng, I.M. Reaney, G.D.C. Csete de Györgyfalva, R. Ubic, J. Yarwood, M.P. Seabra, V.M. Ferreira, Raman spectroscopy of $CaTiO_3$-based perovskite solid solutions, J. Mater. Res. 19 (2011) 488–495.
[28] R.D. Shannon, Revised effective ionic radii and systematic studies of interatomic distances in halides and chalcogenides, Acta Crystallogr. Sect. A 32 (1976) 751–767.
[29] F. Galasso, J. Pyle, Preparation and study of ordering in $A(B'_{0.33}Nb_{0.67})O_3$ perovskite-type compounds, J. Phys. Chem. 67 (1963) 1561–1562.
[30] L. Bellaiche, D. Vanderbilt, Electrostatic model of atomic ordering in complex perovskite alloys, Phys. Rev. Lett. 81 (1998) 1318.
[31] A. Jacobson, B. Collins, B. Fender, A powder neutron and X-ray diffraction determination of the structure of $Ba_3Ta_2ZnO_9$: an investigation of perovskite

Please cite this article in press as: A. Sayyadi-Shahraki, et al., Effect of non-stoichiometry on the densification, phase purity, microstructure, crystal structure, and dielectric loss of $Ba(Co_{1/3}Nb_{2/3})O_3$ ceramics, *J Eur Ceram Soc* (2017), http://dx.doi.org/10.1016/j.jeurceramsoc.2017.04.023

phases in the system Ba–Ta–Zn–O and the preparation of $Ba_2TaCdO_{5.5}$ and $Ba_2CeInO_{5.5}$, Acta Crystallogr. Sect. B 32 (1976) 1083–1087.
[32] H. Wu, P.K. Davies, Influence of non-stoichiometry on the structure and properties of $Ba(Zn_{1/3}Nb_{2/3})O_3$ microwave dielectrics: i. substitution of $Ba_3W_2O_9$, J. Am. Ceram. Soc. 89 (2006) 2239–2249.
[33] J. Bian, G. Song, K. Yan, Structure and microwave dielectric properties of $Ba_{1+x}[(Co_{0.7}Zn_{0.3})_{1/3}Nb_{2/3}]O_3$ ($-0.015 \leq x \leq 0.015$), J. Eur. Ceram. Soc. 27 (2007) 2817–2821.
[34] O. Ovchar, D. Durylin, A. Belous, B. Jancar, A-site deficient perovskites $Ba(M^{2+}{}_{1/3}Nb_{2/3})O_3$: microstructural attributes for a high quality factor, Mater Sci Poland 29 (2011) 56–62.
[35] O. Ovchar, D. Durilin, A. Belous, B. Jančar, T. Kolodiazhnyi, Dielectric and relaxor properties of $Ba_9MNb_{14}O_{45}$ ceramics, J. Am. Ceram. Soc. 95 (2012) 3202–3206.
[36] K.P. Surendran, M.T. Sebastian, P. Mohanan, R.L. Moreira, A. Dias, Effect of nonstoichiometry on the structure and microwave dielectric properties of $Ba(Mg_{0.33}Ta_{0.67})O_3$, Chem. Mater. 17 (2005) 142–151.

Please cite this article in press as: A. Sayyadi-Shahraki, et al., Effect of non-stoichiometry on the densification, phase purity, microstructure, crystal structure, and dielectric loss of $Ba(Co_{1/3}Nb_{2/3})O_3$ ceramics, *J Eur Ceram Soc* (2017), http://dx.doi.org/10.1016/j.jeurceramsoc.2017.04.023